Available online at www.sciencedirect.com
ScienceDirect
Infrared Physics & Technology 50 (2007) 187–190
INFRARED PHYSICS & TECHNOLOGY
www.elsevier.com/locate/infrared

MBE grown type-II MWIR and LWIR superlattice photodiodes

Cory J. Hill *, Jian V. Li, Jason M. Mumolo, Sarath D. Gunapala

Jet Propulsion Laboratory, California Institute of Technology, 4800 Oak Grove Dr., Pasadena, CA 91109, USA

Available online 6 December 2006

Abstract

We report on the status of GaSb/InAs type-II superlattice diodes grown and fabricated at the Jet Propulsion Laboratory designed for infrared absorption 2–5 μm and 8–12 μm bands. Recent LWIR devices have produced detectivities as high as 8×10^{10} Jones with a differential resistance–area product greater than 6 Ohm cm^2 at 80 K with a long wavelength cutoff of approximately 12 μm. The measured internal quantum efficiency of these front-side illuminated devices is close to 30% in the 10–11 μm range. MWIR devices have produced detectivities as high as 8×10^{13} Jones with a differential resistance–area product greater than 3×10^7 Ohm cm^2 at 80 K with a long wavelength cutoff of approximately 3.7 μm. The measured internal quantum efficiency of these front-side illuminated MWIR devices is close to 40% in the 2–3 μm range at low temperature and increases to over 60% near room temperature.

Keywords: Molecular beam epitaxy; Superlattices; Infrared detectors; Infrared photodiodes; Chemical passivation

1. Introduction

The closely lattice-matched material system of InAs, GaSb, and AlSb, commonly referred to as the 6.1 Å material system, has emerged as a fertile ground for the development of new solid-state devices. The flexibility of the system in simultaneously permitting type-I, type-II staggered, and type-II broken-gap band alignments has been the basis for many novel, high-performance heterostructure devices in recent years, including the GaInSb/InAs type-II strained layer superlattice infrared detectors proposed by Smith and Mailhiot [1] in 1987. The type-II superlattice design promises optical properties comparable to HgCdTe, better uniformity, reduced tunneling currents, suppressed Auger recombination, and normal incidence operation [2,3]. In 1990, Chow and co-workers first reported $Ga_{1-x}In_xSb$/InAs superlattice materials with high structural quality, LWIR photoresponse, and LWIR photoluminescence [4]. More recently, in 1997 researchers from Fraunhofer Institute demonstrated good detectivity (approaching HgCdTe, 8-μm cutoff, 77 K) on individual devices [5].

As illustrated in Fig. 1, the band-gap of a type-II superlattice (SL) is determined by the energy separation between the first electron miniband and the top-most hole miniband, rather than the band-gap of a bulk material. Hence, the SL structure can, in principle, be tailored by adjusting constituent layer thicknesses and compositions to cover a wide wavelength range for infrared detection.

In the type-II SL, heavy-holes are largely confined to the GaInSb layers and electrons are primarily confined to the InAs layers. However, because of the relatively low electron mass in InAs, the electron wavefunctions extend considerably beyond the interfaces and have significant overlap with hole wavefunctions. Hence, significant absorption is possible at the minigap energy (shown in Fig. 1 with the vertical arrow) which is tunable by changing layer thickness. It is also possible to obtain large optical absorption coefficients at cutoff wavelengths as long as ~20 μm by taking advantage of internal lattice-mismatch-induced strains in the InAs/GaInSb SLs [2]. Additionally, since the gap of each constituent bulk material is larger than the effective direct gap of the superlattice, dark currents are suppressed in comparison with their values

* Corresponding author. Tel.: +1 818 393 7121; fax: +1 818 393 4540.
E-mail address: cory.j.hill@jpl.nasa.gov (C.J. Hill).

1350-4495/$ - see front matter © 2006 Published by Elsevier B.V.
doi:10.1016/j.infrared.2006.10.033

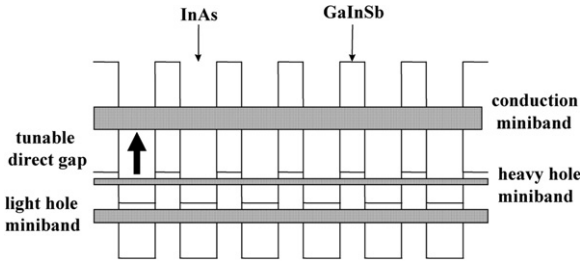

Fig. 1. Schematic of the direct band-gap arising from the conduction and valence minibands in the GaInSb/InAs type-II superlattices.

in similar cutoff wavelength bulk ternary alloys. Another benefit of this structure for detector applications is that normal incidence absorption is permitted by selection rules, obviating the need for grating structures or corrugations that are needed in alternative quantum-well infrared photodetectors (QWIPs) [6]. Finally, Auger transition rates, which place intrinsic limits on the performance of such detectors and severely impact the lifetimes found in the bulk, narrow-gap detectors, can be reduced by judicious choices for the structure's geometry and strain profile [7].

Despite these advantages, there are still several challenges confronting the application of type-II superlattices as narrow-gap photodiodes, with the largest being the growth of thick, high quality strained layer superlattices and achieving an effective reduction of surface leakage currents and band-to-band as well as defect-assisted tunneling currents. Early experimental results on such structures have shown great promise. For example, Fuchs and co-workers from the Fraunhofer Institute have demonstrated type-II InAs/GaInSb photodiodes having cutoff wavelengths ranging from 7.5 to 12 μm with performance characteristics similar to those obtained from HgCdTe-based diodes and argued that improvements in material and device quality would significantly enhance device performance [5]. Recent works have demonstrated high-performance superlattice based imaging arrays [8] and high temperature operation [9] in the 3–5 μm region as well as performance rivaling MCT in the 7–12 μm region [10].

2. Device growth

Superlattice photodiodes were grown in a Veeco Applied-Epi Gen III molecular beam epitaxy chamber equipped with valved cracking sources for the group V Sb_2 and As_2 fluxes, as wells as dual In sources for independently varying the growth rates of GaInSb and InAs. Growth was performed on 50 mm diameter unintentionally doped p-type GaSb (100) substrates. During growth the substrates were separated from the molybdenum wafer holders by a 50 mm outer-diameter pyrolytic boron nitride ring in front and a sapphire backing plate in back. The device recipe is similar to that reported by Razeghi and coworkers [11] and consists of a 0.5 μm Be-doped GaSb buffer layer, followed by a p–i–n superlattice 22 ÅGaSb/48 ÅInAs (LWIR) or 22 ÅGaSb/18 ÅInAs (MWIR) with the first 80 periods Be doped in the GaSb layers, 200 undoped periods, and the final 80 periods doped with Te in the InAs layers. The device is capped with a thin (200–300 Å) layer of n-type InAs.

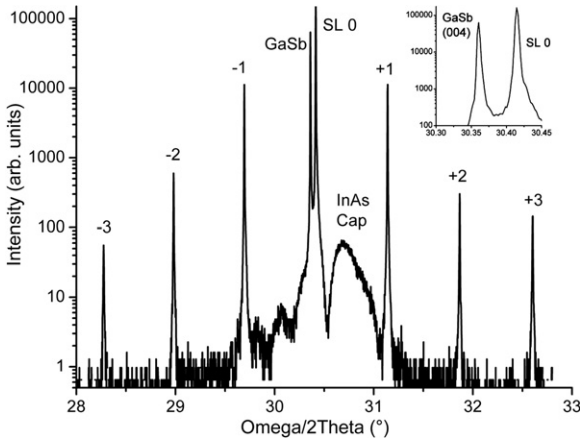

Fig. 2. XRD scan of the superlattice diode near the GaSb (004) reflection. (Inset) Close-up of the substrate and zero-order superlattice peaks.

Fig. 2 shows a typical X-ray diffraction scan of the 22 ÅGaSb/48 ÅInAs device structure near the 004 reflection of the GaSb substrate. The overall periodicity of the structure as measured by the fringe spacing of the superlattice peaks is 70.8 Å, in good agreement with the recipe. The high structural quality of the epilayers is evidenced by the multiple sharp satellite peaks as well as the Pendellosung fringes from the thin InAs cap layer. The cross-sectional transmission electron microscopy (TEM) image of the wafer in Fig. 3 shows no structural defects related to interface dislocations or strain relaxation during the growth of the superlattice layer.

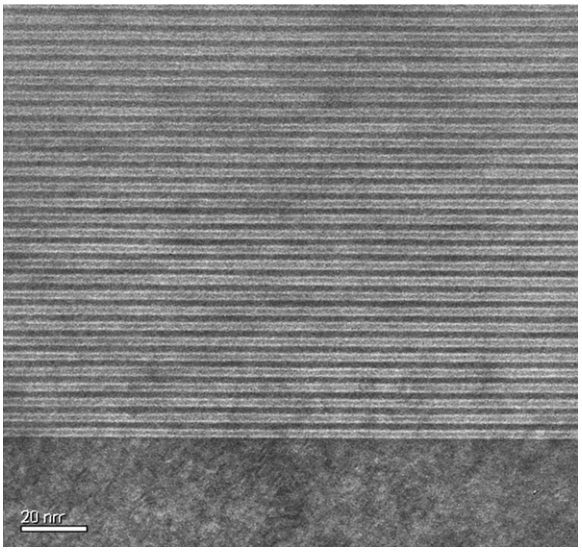

Fig. 3. Typical cross-sectional TEM image of the type-II superlattice on the GaSb buffer layer.

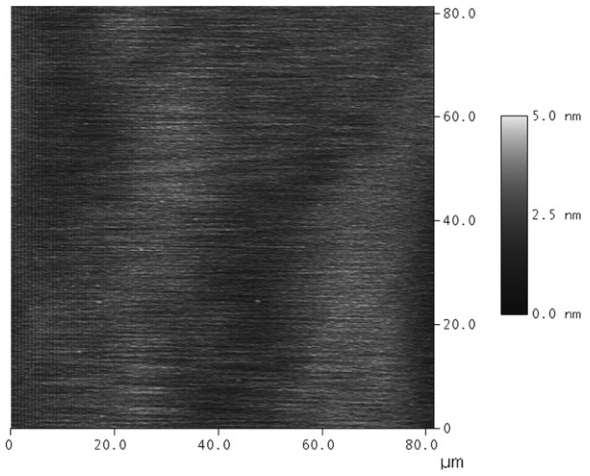

Fig. 4. Large area AFM image of the surface of the as-grown wafer.

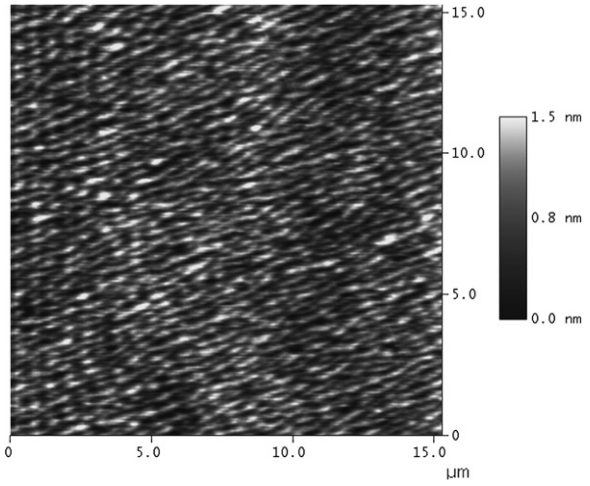

Fig. 5. High-resolution AFM image of the surface of the as-grown wafer.

Fig. 4 shows an atomic force microscope (AFM) scan of the surface of the as-grown epitaxial structure. The surface is very smooth, and typically no large defects are visible on an 80×80 μm scan of the wafer surface, showing a large improvement over our previous samples [12]. Fig. 5 shows a higher-resolution 15×15 μm scan of the wafer surface, showing a very smooth surface on the nano-scale, where the image contrast comes mainly from monolayer steps on the surface. From Fig. 5 a mean surface roughness of 2.5 Å can be extracted. Optical microscopy of the wafer surface reveals a density of roughly 200/cm^2 of micron or larger sized defects. This density of large defects is entirely within the acceptable range for this type of epitaxial growth, and does not preclude the material from being suitable for focal plane array applications.

3. Device processing

Standard contact photolithographic techniques were used to pattern 250×250 μm large area test detectors on the MBE-grown wafers. Samples were wet-etched using a mixture of citric acid, phosphoric acid, and hydrogen peroxide diluted in deionized water at a rate of approximately 400 Å/min in the superlattice region. The etching solution was agitated with a magnetic stirrer to improve uniformity, and the etch process was terminated once the p-GaSb buffer layer was reached. Ti/Pt/Au metal was then evaporated onto the sample to form both the n- and p-type contacts. No post-processing passivation techniques were applied to the devices reported here.

4. Results

Fig. 6 shows the dark-current IV characteristics for a typical 12 μm cutoff 250×250 μm test device measured at 80 K. The RoA value extracted from this 80 K curve is 5.2 Ohm cm^2. Over 70% of devices fabricated in this lot had measured RoA values exceeding 2 Ohm cm^2, with a maximum measured RoA of 6.3 Ohm cm^2. The detectivity, responsivity and quantum efficiency of a typical 12 μm cutoff device measured at 80 K is shown in Fig. 7. The device

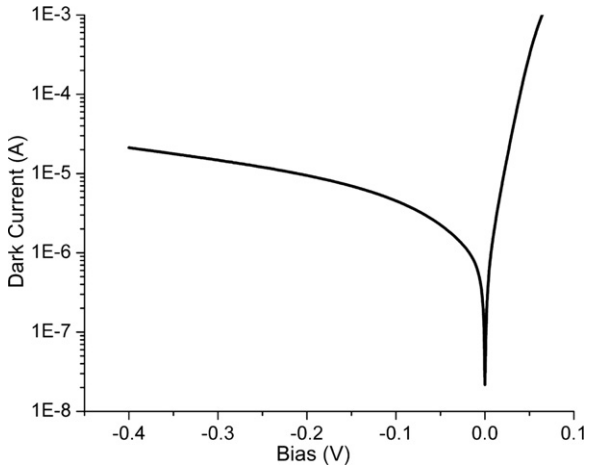

Fig. 6. Dark current vs. applied bias for a typical 12 μm cutoff 250×250 μm test device at 80 K.

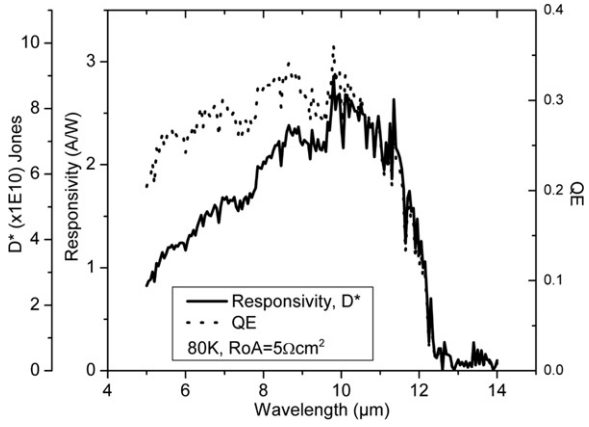

Fig. 7. D^*, responsivity, and QE (dotted, right axis) for the 12 μm cutoff, large-area superlattice photodiodes.

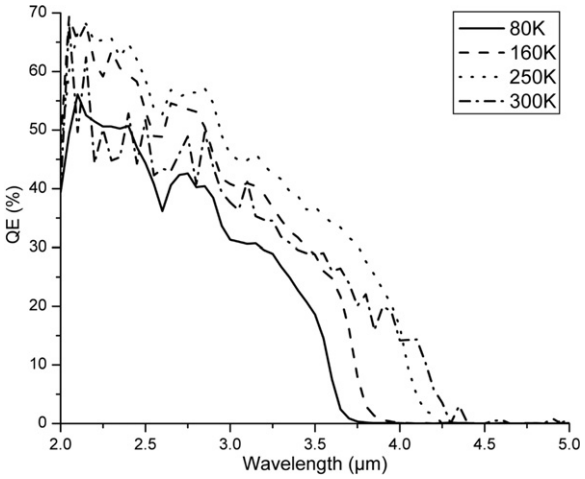

Fig. 8. Quantum efficiency measurements for the large-area MWIR superlattice photodiodes.

responsivity peaks in the 10–11 μm range with a long wavelength cutoff near 12 μm. Our devices were measured with front-side illumination and no antireflective coatings were applied. The detectivity is as high as 8e10 Jones in the 10–11 μm range and the internal QE is nearly 30% in this region as well.

Fig. 8 shows the internal quantum efficiency for the MWIR devices as a function of incident wavelength for various temperatures from 80 K to near room temperature. Corresponding RoA and D^* values for devices tested in this temperature range are given in Fig. 9. Due to the values of RoA and quantum efficiency, these devices have great potential for use in MWIR focal plane applications operating at non-cryogenic temperatures.

5. Summary

We have fabricated and characterized long wavelength infrared photodiodes based on MBE-grown GaSb/InAs superlattices. The material quality of the devices grown was excellent as evidenced by X-ray, TEM and AFM observations. Our devices have demonstrated detectivities as high as 8×10^{10} Jones with a differential resistance–area product greater than 6 Ohm cm^2 at 80 K with a long wavelength cutoff of approximately 12 μm. The measured quantum efficiency of these front-side illuminated devices is near 30% in the 10–11 μm range. MWIR devices have produced detectivities as high as 8×10^{13} Jones with a differential resistance–area product greater than 3×10^7 Ohm cm^2 at 80 K with a long wavelength cutoff of approximately 3.7 μm. The measured internal quantum efficiency of these front-side illuminated MWIR devices is close to 40% in the 2–3 μm range at low temperature and increases to over 60% near room temperature.

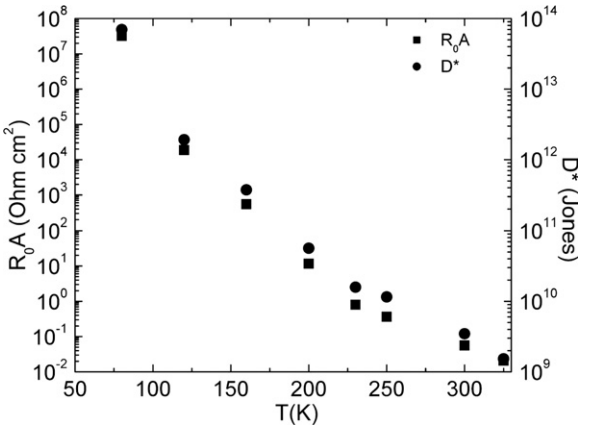

Fig. 9. RoA and D^* values for the large-area MWIR superlattice photodiodes.

Acknowledgements

The authors would like to thank M.Z. Tidrow and P.D. LeVan for their encouragement and guidance in developing antimony-based detectors at the Jet Propulsion Laboratory. The authors are grateful to N. Toomarian, T.N. Krabach, P.J. Grunthaner, S. Forouhar, R. Stirbl, R. Liang, and R. Cox for encouragement and support during the development and optimization of detector arrays at the Jet Propulsion Laboratory for various applications. The research described in this paper was performed by the Jet Propulsion Laboratory, California Institute of Technology, and was sponsored by the Missile Defense Agency.

References

[1] D.L. Smith, C. Mailhiot, J. Appl. Phys. 62 (1987) 2545.
[2] C. Mailhiot, D.L. Smith, J. Vac. Sci. Technol. A 7 (1989) 445.
[3] R.H. Miles, D.H. Chow, in: M. Razeghi (Ed.), Long Wavelength Infrared Detectors, Gordon and Breach, Singapore, 1996, Chapter 7 and references therein.
[4] R.H. Miles, D.H. Chow, J.N. Schulman, T.C. McGill, Appl. Phys. Lett. 57 (1990) 801.
[5] F. Fuchs, U. Weimar, W. Pletschen, J. Schmitz, E. Ahlswede, M. Walther, J. Wagner, P. Koidl, Appl. Phys. Lett. 71 (1997) 3251.
[6] S.D. Gunapala, S.V. Bandara, Semiconduct. Semimet. 62 (2000) 197.
[7] C.H. Grein, P.M. Young, M.E. Flatté, H. Ehrenreich, J. Appl. Phys. 78 (1995) 7143.
[8] M. Walther, R. Rehm, F. Fuchs, J. Schwitz, J. Fleissner, W. Cabanski, D. Eich, M. Finck, W. Rode, J. Wendler, R. Wollrab, J. Ziegler, J. Electron. Mat. 34 (6) (2005) 722–725.
[9] Y.J. Wei, A. Hood, H.P. Yau, A. Gin, M. Razeghi, M.Z. Tidrow, V. Nathan, Appl. Phys. Lett. 86 (2005) 23.
[10] Y. Wei, A. Hood, H. Yau, V. Yazdanpanah, M. Razeghi, M.Z. Tidrow, V. Nathan, Appl. Phys. Lett. 86 (2005) 9.
[11] M. Razeghi, Y. Wei, A. Gin, G.J. Brown, D.K. Johnstone, Proc. SPIE 4650 (2002) 111.
[12] C.J. Hill, S.S. Keo, J.M. Mumolo, S.D. Gunapala, Proc. SPIE (2002) 5783.